Available online at www.sciencedirect.com
SCIENCE DIRECT®
Journal of Power Sources 124 (2003) 174–181
JOURNAL OF POWER SOURCES
www.elsevier.com/locate/jpowsour

Electrochemical characteristics of rancieite-type manganese oxide by mechanochemical synthesis

Sang-gil Woo [a], Hansu Kim [b], Churl Kyung Lee [c], Hun-Joon Sohn [a,*], Tak Kang [a]

[a] School of Materials Science and Engineering, Research Center for Energy Conversion and Storage, Seoul National University, Seoul 151-742, South Korea
[b] Samsung Advanced Institute of Technology, San 14-1, Nongseo-ri, Giheung-eup, Yongin-si, Gyeonggi-do 449-712, South Korea
[c] School of Materials and System Engineering, Kumoh National Institute of Technology, Kumi, Kyungbuk 730-701, South Korea

Received 30 April 2003; accepted 16 May 2003

Abstract

Rancieite-type manganese oxide is synthesized by a mechanochemical method and its electrochemical characteristics as a cathode material for lithium secondary batteries are examined. The discharge capacity increases with milling time up to 45 h with a maximum of 274 mAh g^{-1}. Further increase in milling time causes a decrease in capacity due to a phase transformation. Lithium insertion into the rancieite-type manganese cathode is composed of two processes, one between 2.0 and 4.0 V and the other between 1.5 and 2.0 V. The former is due to the reduction of Mn^{4+} to Mn^{3+}, while the latter is due to the reduction of Mn^{3+} to Mn^{2+}. These processes are identified by X-ray absorption spectra. The specific capacity of the rancieite-type manganese oxide shows good cycleability without transition to a spinel-like structure.

Keywords: Manganese oxide cathode; Lithium-ion battery; Rancieite; Manganese oxide; Mechanochemical synthesis; Soft X-ray absorption

1. Introduction

With increasing demand for potable power sources for electronic equipment, research efforts have been made world-wide over the past decade for lithium-ion rechargeable batteries of higher capacity. Use of lithium-ion batteries for high-power applications requires a high performance cathode material. In this regard, among the many possible oxides of the three-dimensional (3D) transition metals, attention has focused on manganese oxides candidates for lithium intercalation cathode materials. This because such oxides are more abundant, less expensive and more environmentally friendly than the cobalt oxide which is presently used in commercial lithium batteries. Many studies have been carried out on crystalline lithium manganese oxides, such as those with a spinel structure ($LiMn_2O_4$) and those with a layered structure ($LiMnO_2$) [1–4].

Lithium insertion into manganese oxide based materials is accompanied by complicated phase transitions and irreversible structural changes upon cycling which lead to severe capacity loss [5–8]. Various research attempts have been performed, not only to develop new types of manganese oxide based compounds but also to improve their electrochemical properties [9–14]. Among the various manganese oxides, layered manganese oxides have attracted much attention because they have a higher initial specific capacity and provide a two-dimensional interstitial space that allows fast kinetics for intercalation/de-intercalation of lithium without major structural modifications [15–17].

A mechanochemical technique has been applied to synthesize powders to be used as electrode materials, since it provides a wide range of material compositions which are difficult to be prepared by other methods, as well as improved cell reversibility and capacity [18–21].

In this paper, rancieited-type layered manganese oxide is prepared by mechanochemical synthesis. The electrochemical properties of the oxide are investigated by means of electrochemical methods and soft X-ray absorption spectroscopy to examine the electronic structural change during lithium intercalation/de-intercalation.

2. Experimental

Rancieite-type manganese oxide was synthesized as follows. Reagent grade $NaMnO_4{\cdot}H_2O$ (>97%; Aldrich) was dried in vacuum at 120 °C for 2 h to remove residual or adsorbed water, and was then mixed with sulfur (99.98%;

* Corresponding author. Tel.: +82-2-880-7226; fax: +82-2-885-9671.
E-mail address: hjsohn@snu.ac.kr (H.-J. Sohn).

0378-7753/$ – see front matter © 2003 Elsevier B.V. All rights reserved.
doi:10.1016/S0378-7753(03)00619-0

Aldrich) as a reducing agent and NaCl as a process control agent. The blended powders were milled under an argon atmosphere using a vibratory mill with a hardened steel vial of 80 cm^3 capacity. The ball-to-powder ratio was 20:1. The powders were washed several times with distilled water to remove the Na_2SO_4 formed during the milling process, followed by drying in vacuum at 150 °C for 12 h. Samples were identified and characterized with an X-ray diffractrometer (MacScience, MXP18A-HF) and a scanning electron microscope (JEOL, JSM-T200). Thermogravimetric analysis (TGA) of the sample was performed under a nitrogen atmosphere from room temperature to 800 °C at 10 °C/min. The amounts of Na and Mn in the oxide were analyzed using ICP-atomic emission spectroscopy. Finally, the average degree of oxidation of manganese ion within the oxide was determined by chemical titration [11].

The product was mixed with 20 wt.% carbon (Super-P) as a conductor and 8 wt.% polytetrafluoroethylene (pvdf) as a binder. Coin-type cells were assembled in an argon-filled glove box using Celgard 2400 as a separator, 1 M LiPF6, ethylene carbonate (EC)/diethyl carbonate (DEC) (1:1 (v/v); Merck) as an electrolyte, and Li foil as counter and reference electrodes. All cells were tested galvanostatically between 1.5 and 4.0 V versus Li/Li^+.

The manganese L-edge and oxygen K-edge X-ray absorption spectra were obtained with the samples at each specified electrochemical condition. The measurements were performed on a U7 beamline at a storage ring of 2.5 GeV with a ring current of 120–160 mA at the Pohang Light Source in Korea.

3. Results and discussion

X-ray diffraction patterns of samples after different milling times are shown in Fig. 1. After 6 h of milling (Fig. 1(b)), Mn_3O_4 is a major phase, and transforms into Mn_2O_3 after 12 h of milling (Fig. 1(c)), although rancieite-type manganese oxide is clearly visible in both cases. The product after 24 h of milling, as shown in Fig. 1(d), is layered rancieite-type manganese oxide with an interlayer distance of 7.51 Å similar to that of naturally-occurring birnessites. As milling time increases further, the phase remains the same, while longer milling time leads to a better crystallization of the product [18]. The product shows a larger (0 0 1) '*d*' spacing than that (7.42 Å) reported by Tsuji et al. [22]. Apparently this is because a larger cation, Na^+, lies in the interlayer space instead of the smaller H^+ cation. Also, in Fig. 1, X-ray diffraction

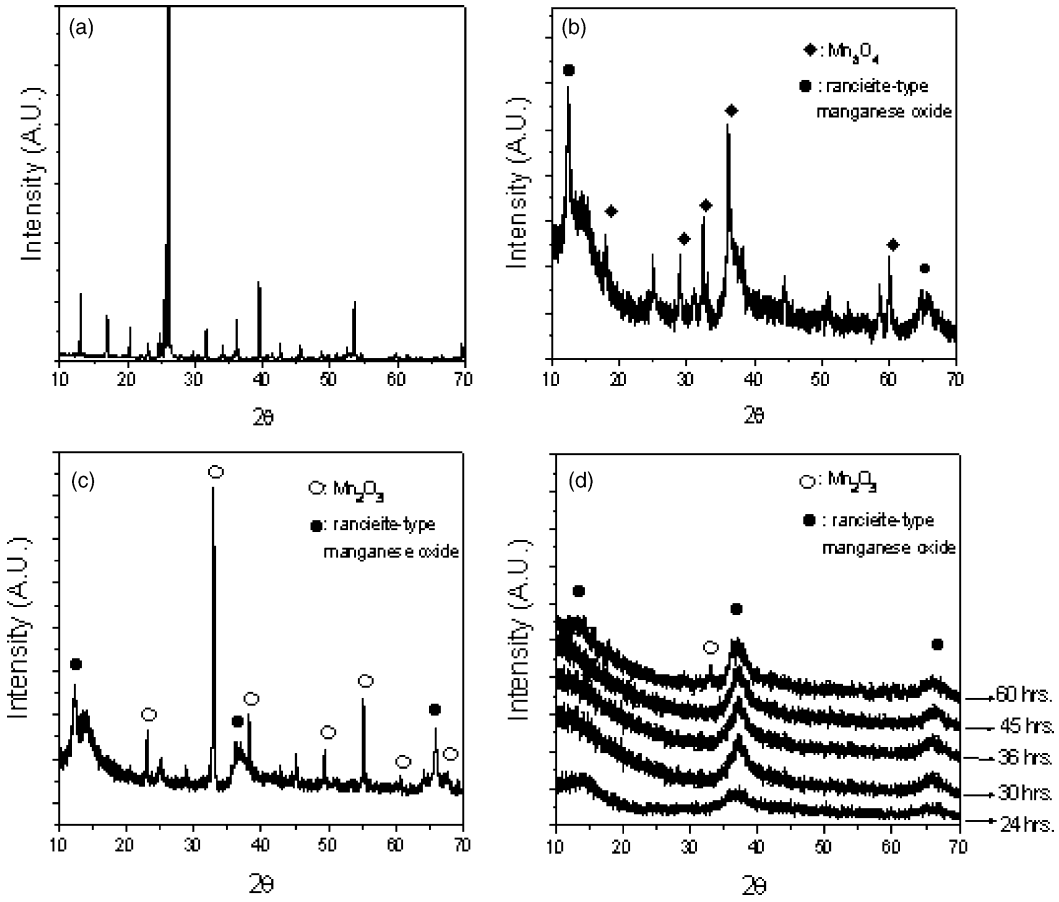

Fig. 1. XRD patterns of samples synthesized by a mechanochemical method as function of milling time. (a) $NaMnO_4$, (b) 6 h, (c) 12 h, (d) 24–60 h.

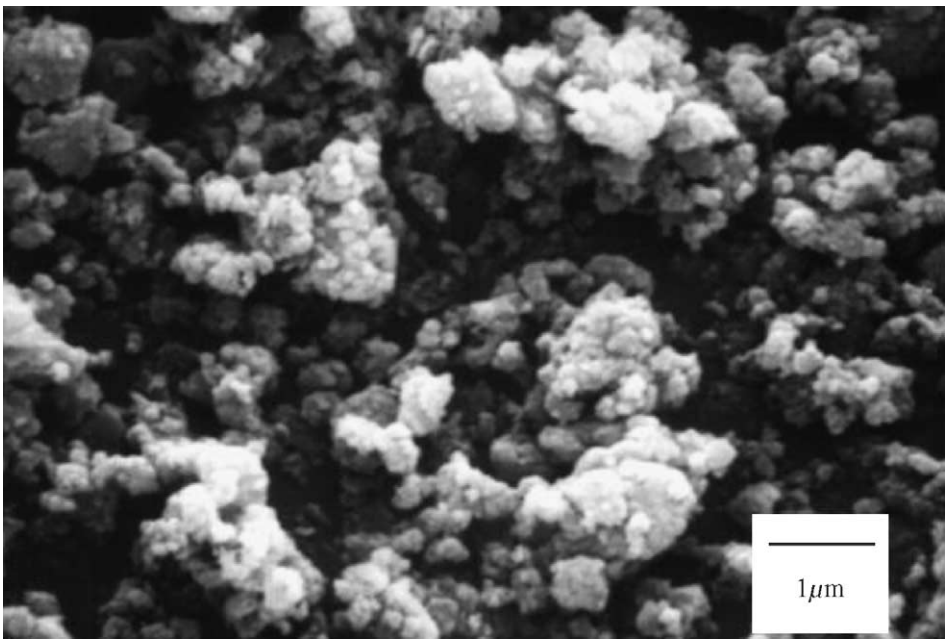

Fig. 2. Scanning electron micrograph of 45-RTMO.

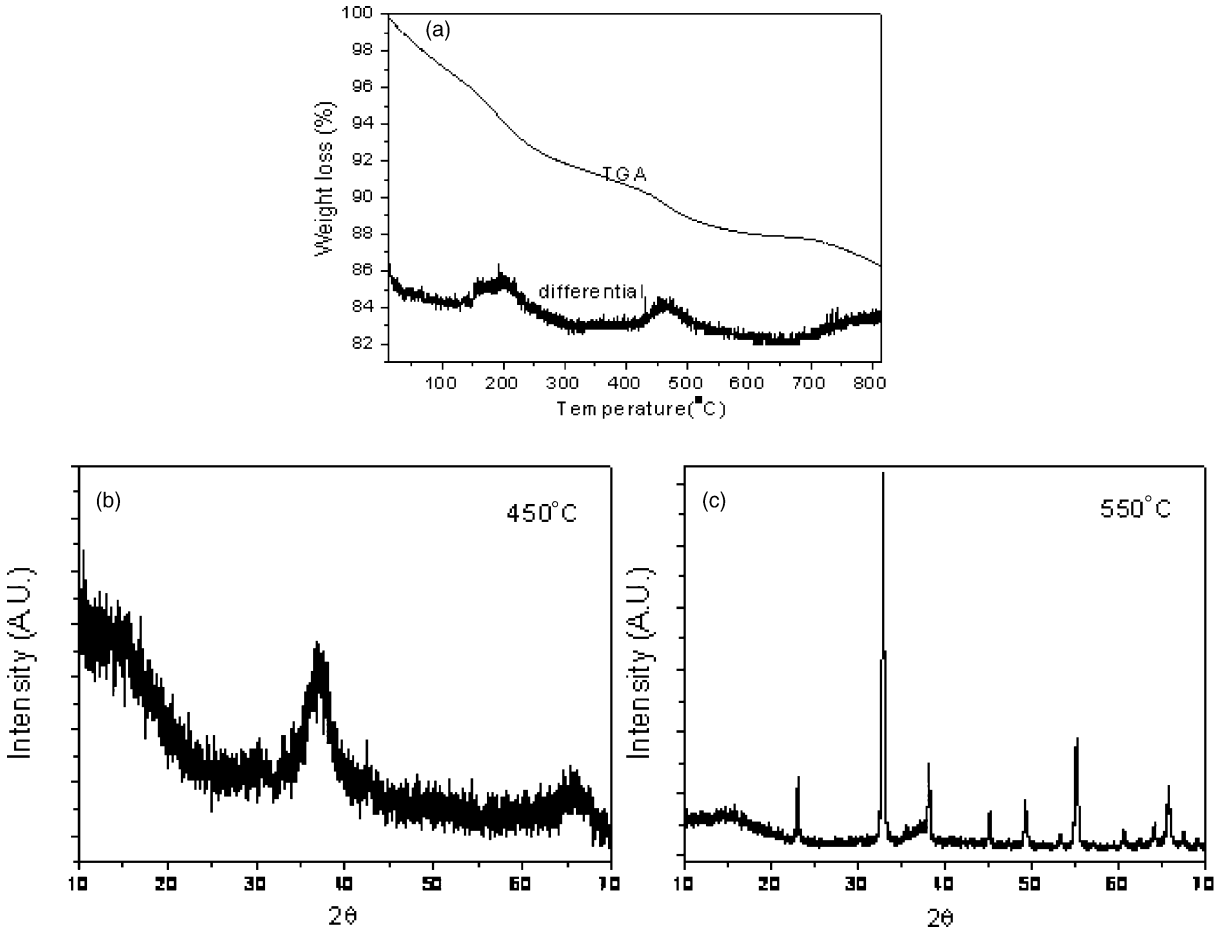

Fig. 3. (a) TGA-curve of 45-RTMO, (b and c) XRD patterns of annealed samples.

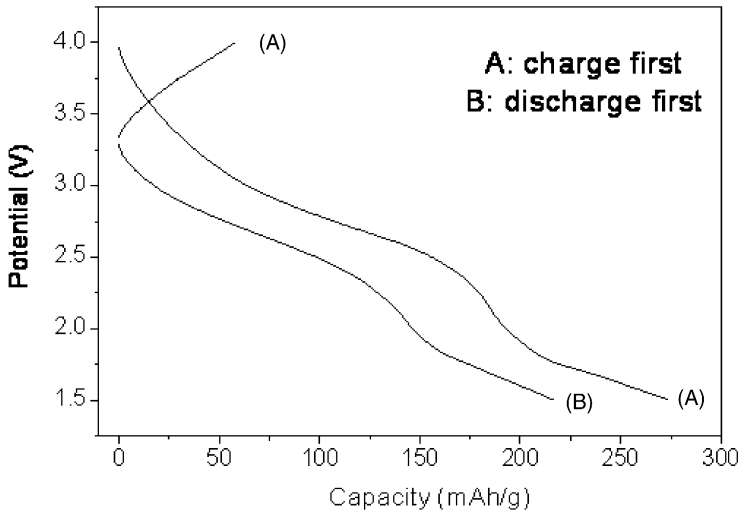

Fig. 4. Voltage profiles of 45-RTMO with different starting mode of charge–discharge.

patterns demonstrate a progressive increase of the oxidation state of manganese, as well as a modification of the oxide stoichiometry, with milling time.

Since rancieite-type manganese oxide synthesized initially contains Na^+ in the interlayer, Na^+ ions are extracted electrochemically first from the lattice to increase Li uptake for cycling experiments. This is discussed later in detail. The first electrochemical discharge capacity (Li insertion) of rancieite-type manganese oxide was measured as a function of milling time. The data were obtained with a current density of 5 mA g^{-1} between 1.5 and 4.0 V. The specific capacities of rancieite-type manganese oxide with 24, 30 and 45 h of milling time were 218, 235 and 274 mAh g^{-1}, respectively. As the milling time increases, the first discharge specific capacity increases to a maximum of 274 mAh g^{-1}. This is probably due to an increase in crystallinity of the rancieite-type oxide material, as shown in Fig. 1(d). By contrast, the capacity of manganese oxide after 60 h of milling time decreases to 173 mAh g^{-1} since the occurrence of the Mn_2O_3 phase leads to a decrease in capacity. Thus, all the following analyses were performed with rancieite-type manganese oxide after 45 h of milling (termed: 45-RTMO), since it displays a better electrochemical behaviour than the others.

A scanning electron micrograph of 45-RTMO is presented in Fig. 2 and shows highly agglomerated particles with a particle size of less than 1 μm. The thermal properties of 45-RTMO were investigated by thermogravimetry (TG) measurements, as shown in Fig. 3(a). The weight loss is rather fast up to 250 °C due to evaporation of water, but then slows down. Above 450 °C, 45-RTMO undergoes phase transformation by thermal decomposition as follows:

$$MnO_y \rightarrow \frac{1}{2}Mn_2O_3 + \left(\frac{y}{2} - \frac{3}{4}\right)O_2 \quad (1)$$

Therefore, it can be seen that before 450 °C, the continuous weight loss is due to the removal of H_2O from the surface and interlayer, and the weight loss of 2 wt.% above 450 °C may result from the loss of oxygen due to reaction (1). As shown in Fig. 3(b) and (c), the phase of 45-RTMO annealed at 450 °C remains the same, but the sample annealed at 550 °C is transformed into Mn_2O_3. Elemental analyses show that the stoichiometry of 45-RTMO is $Na_{0.21}MnO_{2.04}{\cdot}0.57H_2O$ and the average oxidation number of manganese ion is 3.87.

The discharge capacity after charging with 5 mA g^{-1} is higher than that after discharging first, see Fig. 4. This is because de-intercalation of Na^+ occurs as mentioned previously. Theoretically, this reaction corresponds to an oxidation of $Mn^{3.87+}$ cation to $Mn^{4.08+}$. The charge capacity obtained with 45-RTMO up to 4.0 V is equivalent to 0.22 Li per Mn (57.691 mAh g^{-1}) which is close to the theoretical value of 0.21 Li (extracted 0.21 Na^+) per Mn (54.629 mAh g^{-1}). As a result, Na^+ de-intercalation occurs during initial charge and leads to an increase in the subsequent discharge capacity.

Energy dispersive analysis by X-ray (EDAX) shows no sign of Na in the manganese oxide exists on the next dis-

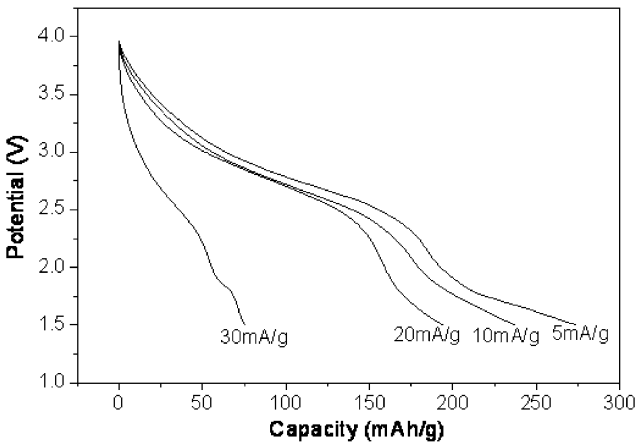

Fig. 5. Voltage profiles for first discharge step of 45-RTMO between 1.5 and 4.0 V as function of current density.

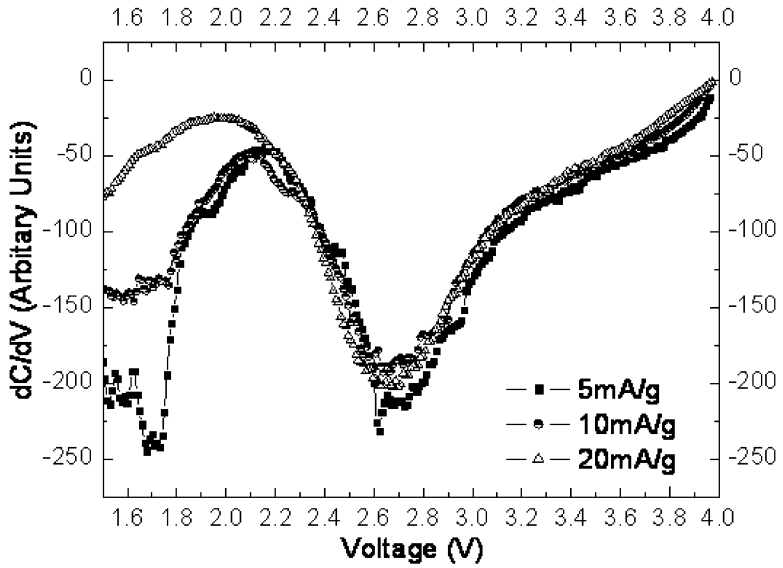

Fig. 6. Differential capacity plots for first discharge step of 45-RTMO as function of current density.

charge. It may therefore be assumed reasonably that the next discharge corresponds to Li intercalation within the structure. Therefore, all electrochemical tests have been performed after initial charging up to 4.0 V [15,23,24].

Voltage profiles for the first discharge step from 4.0 to 1.5 V of 45-RTMO at four different current densities are given in Fig. 5. 45-RTMO at a low current of 5 mA g^{-1} exhibits an extremely high specific capacity of 274 mAh g^{-1}, which corresponds to an insertion of 0.97 Li per Mn. The higher current rate, the lower is the discharge capacity. This is probably due to diffusion limitations. All the electrochemical discharge curves show no distinct plateaux, which indicates the characteristic of a topotactic single-phase reaction. In addition, the smooth discharge curve with a uniform slope may provide the advantage of avoiding problems that may occur with overdischarging or overcharging [9].

Differential capacity plots of the first discharge process at various current densities between 1.5 and 4.0 V are presented in Fig. 6. These curves show two main processes, one between 2.5 and 2.8 V and the other between 1.5 and 1.8 V. Characterization of this differential capacity plot will be addressed in the following discussion, together with the X-ray

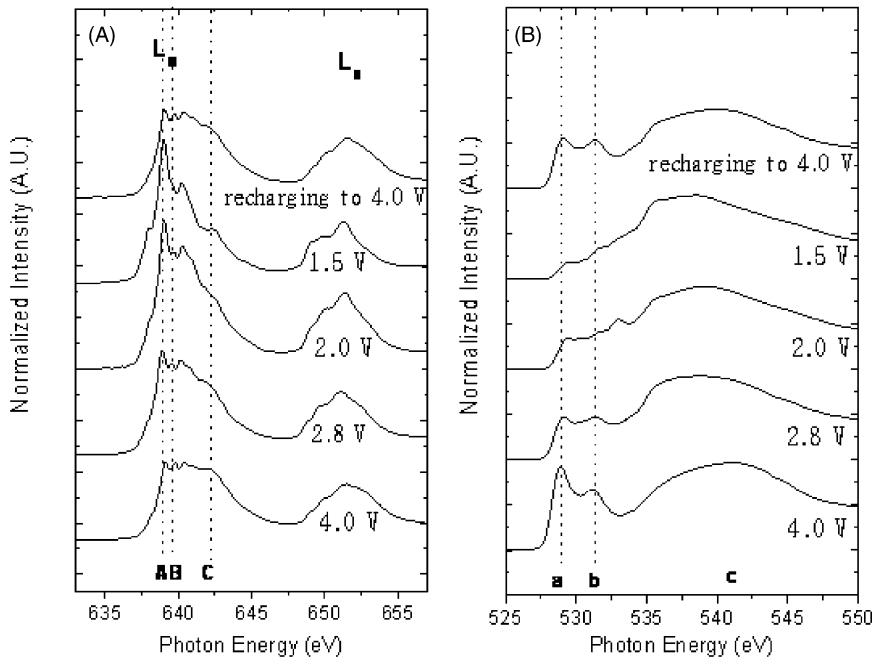

Fig. 7. (a) Mn L_{III} and L_{II}-edge XAS spectra and (b) O K-edge XAS spectra of 45-RTMO during first cycle.

Table 1
Composition of energies of Mn L_{III}-edge peaks (A, B, C) in 45-RTMO measured in this study and in [28]

This work		[28]	
Peak position	Manganese L_{III} peak (eV)	Manganese oxides	Manganese L_{III} peak (eV)
A	639.1	MnO (Mn^{2+})	639.0
B	639.7	Mn_2O_3 (Mn^{3+})	639.6
C	642.1	MnO_2 (Mn^{4+})	642.1

absorption spectroscopy (XAS) data obtained at a current density of 20 mA g^{-1}.

The electronic structure of manganese ion in 45-RTMO during lithium intercalation/de-intercalation have been investigated qualitatively with peak features of Mn $L_{II,III}$-edge X-ray absorption spectroscopy, because the peak shapes and chemical shifts are very sensitive probe of the oxidation state, spin state, and bond covalency [25,26]. The Mn L_{III} and L_{II}-edge XAS spectra of 45-RTMO are shown in Fig. 7(a) with respect to discharge–charge voltage during the first cycle. The Mn absorption peak near 638–644 eV relates to the $2p_{3/2}$ (L_{III}) edge and that near 650–654 eV to the $2p_{1/2}$ (L_{II}) edge peak. The spectral line shapes of the Mn L_{III}-edge of 45-RTMO charged initially to 4.0 V are complicated by the presence of various oxidation states of manganese ions (Fig. 7(a)). As shown in Table 1, the positions A, B and C of the complicated peaks of L_{III}-edge features are in a good agreement with those of the Mn ion in different oxidation states obtained by Paterson and Krivanek [27]. In this case, the A, B and C peaks correspond to the main peaks in Mn^{2+}, Mn^{3+} and Mn^{4+}, respectively. With Li-intercalation from 4.0 to 2.0 V, the relative intensities of the A and B peaks increase, while the relative intensity of C peak decreases. With intercalation from 2.0 to 1.5 V, however, the intensity of peak A increases, but the relative intensities of peaks B and C decreases. The variation of peak intensity with electrochemical discharge can be explained in terms of two main processes of Li-intercalation, a shown in differential capacity plots (Fig. 6). The process for Li-intercalation from 4.0 to 2.0 V is due to the reduction of Mn^{4+} to Mn^{3+}, while the process for Li-intercalation from 2.0 to 1.5V involves reduction of Mn^{3+} to Mn^{2+}, which is consistent with the data reported by Leroux et al. [15]. The relative intensities of peaks A, B and C become almost the same as the initial peak (bottom spectra) upon charging to 4.0 V, which indicates that the charge–discharge process is fairly reversible.

The O K-edge XAS of 45-RTMO with respect to the degree of Li-ion intercalation is given in Fig. 7(b). The spectrum of 45-RMTO charged to 4.0 V presents relatively sharp, doublet peaks a at 529 eV, and b at 531 eV and a broad and higher energy peak c over 536 eV. Peaks a and b correspond to the transition of the oxygen 1s electron to the hybridized states of the Mn 3d ($2t_{2g}$ and $3e_g$) orbital and the oxygen 2p orbital, whereas peak c involves transition to the hybridized states of Mn 4sp and oxygen 2p orbitals [28,29]. The relative intensities of peaks a and b weaken gradually with Li-intercalation from 4.0 to 1.5 V. The reappearance of these peaks is shown upon charging to 4.0 V. Consequently, the weakening of the intensities of peaks a and b reflects an increase of 3d electrons and a decrease in the manganese oxidation state, as discussed above.

From the differential capacity plots (Fig. 6) and XAS spectra (Fig. 7), it is found that the process for Li-intercalation from 2.0 to 1.5 V, which involves reduction of Mn^{3+} to Mn^{2+}, is highly sensitive to the current applied. As shown in Fig. 6, the intensity of the discharge peak at 2.7 V, where the reduction of Mn^{4+} to Mn^{3+} occurs, hardly changes with the current density. By contrast, it decreases as the current density increases during the reduction of Mn^{3+} to Mn^{2+} near 1.7 V. Therefore, the reduction of Mn^{3+} to Mn^{2+} appears relatively difficult at higher current density due to diffusion limitations which lead to a lower capacity.

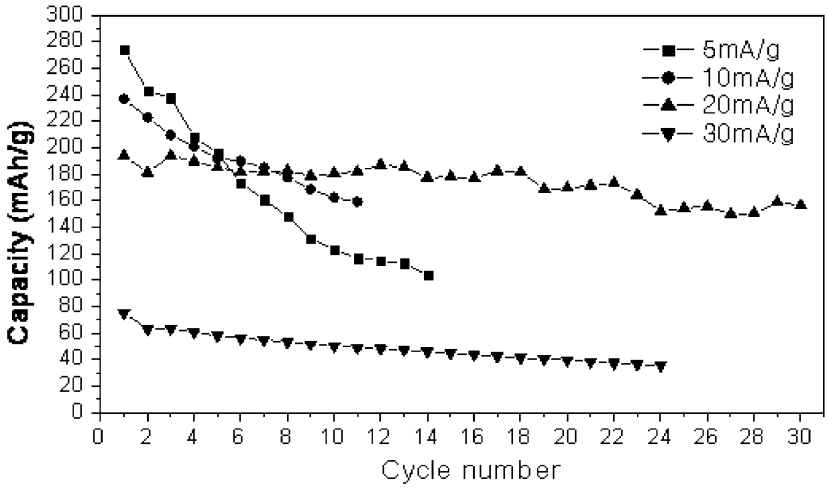

Fig. 8. Cycle performance of 45-RTMO between 1.5 and 4.0 V as function of current density.

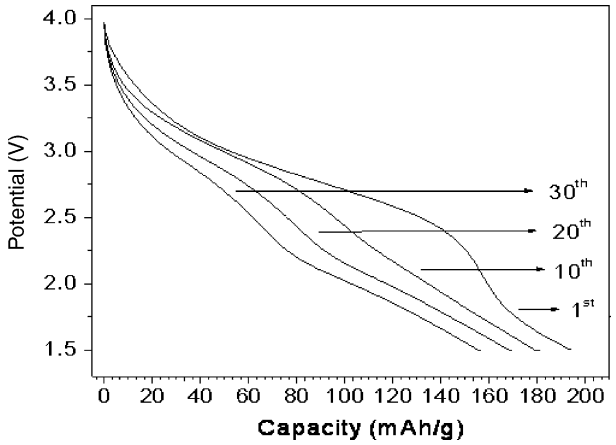

Fig. 9. Discharge voltage profiles for 1st, 10th, 20th, and 30th cycles of 45-RTMO at 20 mA g^{-1} between 1.5 and 4.0 V.

The cycling behaviour of 45-RTMO at various current densities between 1.5 and 4.0 V is given in Fig. 8. At the lowest current density of 5 mA g^{-1}, the capacity decreases rapidly as has been found with most layered manganese oxides. At a current density of 20 mA g^{-1}, however, 45-RTMO demonstrates good capacity retention. Although the initial capacity is lower at 20 mA g^{-1}, 45-RTMO good cycleability without severe fading of capacity for at least 30 cycles (about 81% of initial capacity).

As reported earlier [5,8], the capacity loss in layered manganese oxide is attributed partly to a diffusion of manganese from the Mn occupancy to the Li tetrahedral layer during cycling, which leads to spinel or spinel-like phases. Upon repeated cycling, however, the voltage profile of 45-RTMO at 20 mA g^{-1} (Fig. 9) does not show any tendency to evolve the 4 or 3 V plateaux which would represent a transition to a spinel or spinel-like phase. Therefore, for charge–discharge cycling of 45-RTMO at 20 mA g^{-1}, such transition is absent and structural modification due to the intercalation of Li is less severe than that at a lower current rate.

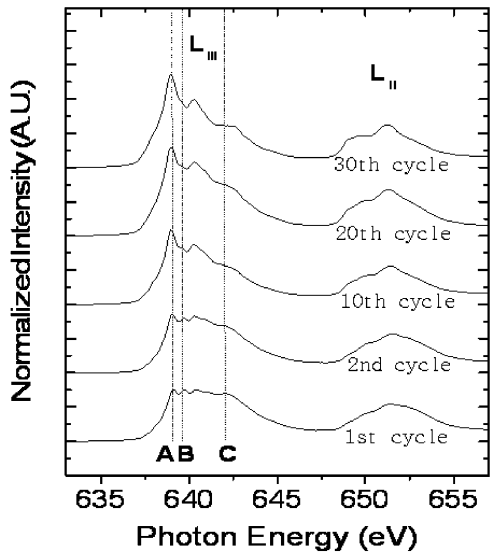

Fig. 10. Mn L_{III} and L_{II}-edge XAS spectra of 45-RTMO charged to 4.0 V as function of cycle number.

The above conclusion is confirmed by the Mn L_{III} and L_{II}-edge XAS spectra with respect to cycling (Fig. 10). Upon cycling, the relative intensity of peak A increases continuously while that of peak C decreases gradually. Peak B remains mostly unaffected by Li intercalation /de-intercalation process. The overall spectra of the Mn L_{III} and L_{II}-edge have similar multiplet oxidation states with three appreciable peaks, and have a similar separation width between L_{III} and L_{II}-edge in spite of cycling. Thus, upon repeated cycling, although the slight capacity fading attributes to a small irreversible part of the reduction of Mn^{3+} to Mn^{2+}, the existence of Mn^{3+} and Mn^{4+} ions leads to improved capacity retention for at least 30 cycles. In addition, this indicates that a 45-RTMO cathode cycled at high current density smoothly accommodates the distortion without producing a macroscopic phase transition, which leads good capacity retention.

4. Conclusions

Rancieite-type manganese oxide has been synthesized using a mechanochemical method to be used as a cathode material for a lithium rechargeable battery. Powders produced after 45 h of milling show a high specific capacity of 274 mAh g^{-1} on discharging at a current density of 5 mA g^{-1} between 1.5 and 4.0 V. Although discharging at high current density (20 mA g^{-1}) presents a lower specific capacity of 194 mAh g^{-1}, there is no transition to a spinel-like structure cycling. This results in an improved specific capacity retention of about 81% of initial capacity even after 30 cycles. This performance is confirmed by differential capacity plots and X-ray absorption spectra.

Acknowledgements

Experiments at the Pohang Light Source (PLS) were supported in part by MOST and POSCO. The authors wish to thank the authorities at the PLS for help with XAS measurements. The project was supported by KOSEF through the Research Center for Energy Conversion and Storage at Seoul National University.

References

[1] M. Tabuchi, K. Ado, H. Kobayashi, H. Kageyama, C. Masquelier, A. Kondo, R. Kanno, J. Electrochem. Soc. 145 (1998) L49.
[2] S. Bach, J.P. Pereira-Ramos, N. Baffier, J. Electrochem. Soc. 143 (1996) 3429.
[3] R.J. Gummow, A. de Kock, M.M. Thackeray, Solid State Ion. 69 (1994) 59.
[4] J.M. Tarascon, D. Guyomard, Electrochim. Acta 38 (1993) 1221.

[5] J. Reed, G. Ceder, A. Van der Ven, Electrochem. Solid-State Lett. 4 (6) (2001) A78.
[6] Y. Xia, H. Noguchi, M. Yoshio, J. Solid State Chem. 119 (1995) 216.
[7] J.M. Tarascon, W.R. McKinnon, F. Coowar, T.N. Bowmer, G. Amatucci, D. Guyomard, J. Electrochem. Soc. 141 (1994) 1421.
[8] R. Chen, M. Stanley Whittingham, J. Electrochem. Soc. 144 (1997) L64.
[9] J. Kim, A. Manthiram, Nature 390 (1997) 265.
[10] J.J. Xu, A.J. Kinser, B.B. Owens, W.H. Smyrl, Electrochem. Solid-State Lett. 1 (1998) 1.
[11] N. Kumagai, T. Saito, S. Komaba, J. Appl. Electrochem. 30 (2000) 1.
[12] D. Im, A. Manthiram, J. Electrochem. Soc. 149 (2002) A1001.
[13] S.H. Kang, J.B. Goodenough, K. Rabnberg, Electrochem. Solid-State Lett. 4 (2001) A49.
[14] J.J. Xu, J. Yang, G. Jain, Electrochem. Solid-State Lett. 5 (2002) A223.
[15] F. Leroux, D. Guyomard, Y. Piffard, Solid State Ion. 80 (1995) 307.
[16] B.J. Aronson, A.K. Kinser, S. Passerini, W.H. Wmyrl, A. Stein, Chem. Mater. 11 (1999) 949.
[17] M.M. Thackeray, Prog. Solid State Chem. 25 (1997) 1.
[18] C. Suryanarayana, Prog. Mater. Sci. 46 (2001) 1.
[19] M.N. Obrovac, O. Mao, J.R. Dahn, Solid State Ion. 112 (1998) 9.
[20] S. Soiron, A. Rougier, L. Aymard, M. Tarascon, J. Power Sources 97–98 (2001) 402.
[21] N.V. Kosova, I.P. Asanov, E.T. Devyatkina, E.G. Avvakumov, J. Solid State Chem. 146 (1999) 184.
[22] M. Tsuji, S. Komarneni, Y. Tamaua, M. Abe, Mater. Res. Bull. 27 (1992) 741.
[23] P. Le Goff, N. Baffier, S. Bach, J.P. Pereira-Ramos, R. Messina, Solid State Ion. 61 (1993) 309.
[24] F. Le Cras, S. Rohs, M. Anne, P. Strobel, J. Power Sources 54 (1995) 319.
[25] J.G. Chen, Surf. Sci. Rep. 30 (1997) 1.
[26] A. Ibarra-Palos, P. Strobel, O. Proux, J.L. Hazemann, M. Anne, M. Morcrette, Electrochim. Acta 47 (2002) 3171.
[27] J.H. Paterson, O.L. Krivanek, Ultramicroscopy 32 (1990) 319.
[28] F.M.F. Degroot, M. Grioni, J.C. Fuggle, Phy. Rev. B 40 (1989) 5715.
[29] J.G. Chen, B. Frühberger, M.L. Colaianni, J. Vac. Sci. Technol. A 14 (1996) 1668.